

# Real-time $GW$ : Toward an *ab initio* description of the ultrafast carrier and exciton dynamics in two-dimensional materials

E. Perfetto,<sup>1,2</sup> Y. Pavlyukh,<sup>1</sup> and G. Stefanucci<sup>1,2</sup>

<sup>1</sup>*Dipartimento di Fisica, Università di Roma Tor Vergata, Via della Ricerca Scientifica 1, 00133 Rome, Italy*

<sup>2</sup>*INFN, Sezione di Roma Tor Vergata, Via della Ricerca Scientifica 1, 00133 Rome, Italy*

We demonstrate the feasibility of the time-linear scaling formulation of the  $GW$  method [Phys. Rev. Lett. **124**, 076601 (2020)] for *ab initio* simulations of optically driven two-dimensional materials. The time-dependent  $GW$  equations are derived and solved numerically in the basis of Bloch states. We address carrier multiplication and relaxation in photo-excited graphene and find deviations from the typical exponential behavior predicted by the Markovian Boltzmann approach. For resonantly pumped semiconductor we discover a self-sustained screening cascade leading to the Mott transition of coherent excitons. Our results draw attention to the importance of non-Markovian and dynamical screening effects in out-of-equilibrium phenomena.

In the last two decades the  $GW$  approximation [1] has emerged as a successful and popular tool for describing at microscopic level electronic and optical properties of quantum matter. The merits of this method arise from the proper inclusion of dynamical and non-local effects, leading to band structures and absorption spectra in excellent agreement with experiments in a broad class of materials [2, 3].

The nonequilibrium extension of the  $GW$  approximation to address ultrafast phenomena has been so far computationally prohibitive. The real-time  $GW$  method is based on the numerical solution of the Kadanoff-Baym equations (KBE) for the one-particle Green's function (GF). As the method scales cubically with the physical propagation time [4–6], the  $GW$ –KBE have only been applied to model systems [7–11] and confined to very short time scales [12]. The time-scaling does not improve even within the Generalized Kadanoff-Baym Ansatz (GKBA) [13], and simulations up to few hundreds of femtoseconds have been restricted to jellium-like models [14–16].

A significant advance has been recently achieved with a time-linear scaling formulation of the  $GW$ –GKBA approach [17, 18]. The  $GW$ –GKBA equations have been mapped onto a coupled system of ordinary differential equations (ODE) for the one-particle density matrix and the equal-time 2-particle GF. The ODE scheme (also applicable to second-Born,  $T$ -matrix [17, 18] and other correlated methods [19, 20]) preserves the full non-Markovian nature of the dynamics but it has been so far tested only in small finite systems [17, 18, 20].

In this Letter we extend and solve numerically the  $GW$ –ODE scheme for spatially periodic two-dimensional (2D) systems, thus opening the way to *ab-initio* real-time  $GW$  simulations in material science. We investigate two different materials to highlight different aspects of the  $GW$  method. First we re-examine the problem of carrier multiplication in photo-excited graphene [21–27]. By comparison with Boltzmann equation (BE) results, we show that the (so far neglected) non-Markovian effects modify considerably the impact ionization dynamics. The second application concerns with the photo-generated screening in 2D semiconductors. Pumping resonantly with the exciton energy [28–30], we find that there is

a critical excitation density above which the coherent exciton superfluid melts abruptly (*coherent exciton Mott transition*) well before phonon-induced decoherence takes places [31]. This is due to a self-sustained screening cascade, a phenomenon that can be captured only if the screened electron-hole ( $e$ - $h$ ) attraction is properly updated during the evolution.

*Real-time  $GW$  formalism* – We consider a periodic system with  $N_b$  bands and denote by  $V_{lmni}^{\mathbf{q}\mathbf{k}\mathbf{k}'}$  the scattering amplitude for two electrons in bands  $m$  and  $i$  with quasimomenta  $\mathbf{k}' + \mathbf{q}$  and  $\mathbf{k} - \mathbf{q}$  to end up in the bands  $n$  and  $l$  with quasimomenta  $\mathbf{k}'$  and  $\mathbf{k}$  respectively, see Fig. 1(a). Let us introduce the spin-symmetric lesser and greater GFs  $G_{\mathbf{k}ij}^<(t, t') = i\langle c_{\mathbf{k}j\sigma}^\dagger(t')c_{\mathbf{k}i\sigma}(t) \rangle$  and  $G_{\mathbf{k}ij}^>(t, t') = -i\langle c_{\mathbf{k}i\sigma}(t)c_{\mathbf{k}j\sigma}^\dagger(t') \rangle$ , where  $\hat{c}_{\mathbf{k}i\sigma}^{(\dagger)}$  annihilates (creates) an electron with quasimomentum  $\mathbf{k}$  and spin  $\sigma$  in band  $i$ . The inclusion of spin-orbit and the generalization to spin-dependent GFs is straightforward. The goal of this work is to study the temporal evolution of the one-particle density matrix  $\rho_{\mathbf{k}ij}(t) \equiv -iG_{\mathbf{k}ij}^<(t, t)$  in the  $GW$  approximation. By defining  $\Sigma_{\mathbf{k}}(t, t')$  as the  $GW$  self-energy, see Fig. 1(b), the equation of motion to solve is

$$\frac{d\rho_{\mathbf{k}}(t)}{dt} = -i[h_{\mathbf{k}}(t), \rho_{\mathbf{k}}(t)] - I_{\mathbf{k}}(t) - I_{\mathbf{k}}^\dagger(t), \quad (1)$$

$$I_{\mathbf{k}}(t) = \int dt' [\Sigma_{\mathbf{k}}^>(t, t')G_{\mathbf{k}}^<(t', t) - \Sigma_{\mathbf{k}}^<(t, t')G_{\mathbf{k}}^>(t', t)] \quad (2)$$

where all quantities are  $N_b \times N_b$  matrices in the band indices. The time-dependent single-particle Hamiltonian reads [32]

$$h_{\mathbf{k}ij}(t) = \delta_{ij}\epsilon_{\mathbf{k}i} + P_{\mathbf{k}ij}(t) + \sum_{\mathbf{k}'mn} (2V_{imnj}^{\mathbf{0}\mathbf{k}\mathbf{k}'} - V_{imjn}^{(\mathbf{k}-\mathbf{k}')\mathbf{k}\mathbf{k}'}) \delta\rho_{\mathbf{k}'nm}(t), \quad (3)$$

where the  $\epsilon_{\mathbf{k}i}$  are the band-dispersions of a preliminary *equilibrium*  $GW$  calculation whereas  $P_{\mathbf{k}ij}(t)$  describes the coupling of the electrons to an external field. The last term in Eq. (3) is the variation of the Hartree-Fock potential due to the variation ( $\delta\rho$ ) of the density matrix with respect to the equilibrium value  $\rho_{\mathbf{k}nm}^{\text{eq}} = \delta_{nm}f(\epsilon_{\mathbf{k}n})$ , with  $f$  the zero-temperature Fermi-Dirac distribution.

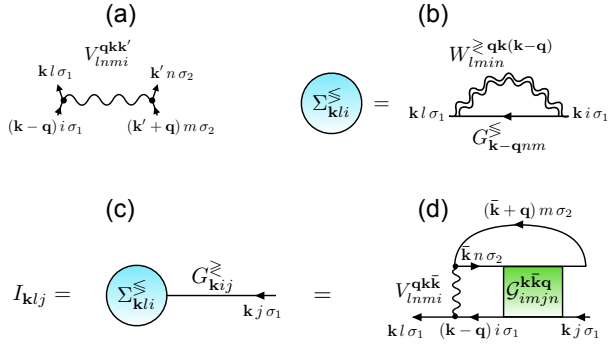


FIG. 1. Diagrammatic representation of the Coulomb scattering amplitude (a),  $GW$  self-energy (b) and collision integral in terms of the self-energy (c), and two-particle GF (d).

We implement the GKBA [13] to obtain a closed equation for  $\rho$ , i.e., we express the lesser and greater GFs as  $G_{\mathbf{k}}^{\lessgtr}(t, t') = -G_{\mathbf{k}}^{\text{R}}(t, t')\rho_{\mathbf{k}}^{\lessgtr}(t') + \rho_{\mathbf{k}}^{\lessgtr}(t)G_{\mathbf{k}}^{\text{A}}(t, t')$ , where we have defined  $\rho_{\mathbf{k}}^{\lessgtr} = \rho_{\mathbf{k}} \pm \mathbb{1}$ . The retarded and advanced propagators are approximated at the quasi-particle level, hence  $G_{\mathbf{k}}^{\text{R}}(t, t') = -i\theta(t-t')T\{e^{-i\int_{t'}^t d\bar{t} h_{\mathbf{k}}(\bar{t})}\}$  ( $T$  being the time-ordering operator) and  $G_{\mathbf{k}}^{\text{A}}(t, t') =$

$[G_{\mathbf{k}}^{\text{R}}(t', t)]^{\dagger}$ . The bottleneck in solving Eq. (1) is the numerical calculation of the  $GW$  self-energy  $\Sigma_{\mathbf{k}ij}^{\lessgtr}(t, t') = i\sum_{\mathbf{q}mn} W_{imjn}^{\lessgtr qk(k-q)}(t, t')G_{\mathbf{k}-\mathbf{q}nm}^{\lessgtr}(t, t')$  since the screened interaction  $W(t, t')$  obeys an RPA-like integral equation for every  $t$  and  $t'$ , making the overall numerical scaling cubic in the propagation time. Remarkably, however, such scaling can be reduced from cubic to linear through the simultaneous propagation of the two-particle GF  $\mathcal{G}$  [17, 18]. The collision integral  $I(t)$  in Eq. (2), see also Fig. 1(c), can equivalently be written in terms of  $\mathcal{G}$  as illustrated in Fig. 1(d):

$$I_{klj}(t) = -i \sum_{\bar{\mathbf{k}}\mathbf{q}} \mathcal{G}_{imjn}^{\mathbf{k}\bar{\mathbf{k}}\mathbf{q}}(t) \mathcal{V}_{ni}^{(-\mathbf{q})\bar{\mathbf{k}}\mathbf{k}}, \quad (4)$$

where  $\mathcal{G}_{lm}^{\mathbf{k}\bar{\mathbf{k}}\mathbf{q}} = \mathcal{G}_{lmim}^{\mathbf{k}\bar{\mathbf{k}}\mathbf{q}}$  and  $\mathcal{V}_{lm}^{\mathbf{q}\bar{\mathbf{k}}\mathbf{k}} = V_{lnmi}^{\mathbf{q}\bar{\mathbf{k}}\mathbf{k}}$  are matrices (two-index tensors) in the space of pairs of band indices [33]. Henceforth we use boldface letters to denote matrices in this space. Introducing also the matrices  $\mathbf{h}_{\mathbf{k}\bar{\mathbf{k}}', lm}(t) \equiv h_{\mathbf{k}lm}(t)\delta_{in} - h_{\mathbf{k}'ni}(t)\delta_{lm}$  and  $\rho_{\mathbf{k}\bar{\mathbf{k}}', lm}^{\lessgtr}(t) \equiv \rho_{\mathbf{k}lm}^{\lessgtr}(t)\rho_{\mathbf{k}'ni}^{\lessgtr}(t)$  we obtain a compact equation of motion for the 2-particle GF [33]:

$$\begin{aligned} i\frac{d}{dt}\mathcal{G}^{\mathbf{k}\bar{\mathbf{k}}\mathbf{q}}(t) = & -2 \left[ \rho_{(\mathbf{k}-\mathbf{q})\mathbf{k}}^{\lessgtr}(t) \mathcal{V}^{\mathbf{q}(\mathbf{k}-\mathbf{q})(\bar{\mathbf{k}}+\mathbf{q})} \rho_{\bar{\mathbf{k}}(\bar{\mathbf{k}}+\mathbf{q})}^{\lessgtr}(t) - \rho_{(\mathbf{k}-\mathbf{q})\mathbf{k}}^{\lessgtr}(t) \mathcal{V}^{\mathbf{q}(\mathbf{k}-\mathbf{q})(\bar{\mathbf{k}}+\mathbf{q})} \rho_{\bar{\mathbf{k}}(\bar{\mathbf{k}}+\mathbf{q})}^{\lessgtr}(t) \right] \\ & + \mathbf{h}_{(\mathbf{k}-\mathbf{q})\mathbf{k}}(t) \mathcal{G}^{\mathbf{k}\bar{\mathbf{k}}\mathbf{q}}(t) - \mathcal{G}^{\mathbf{k}\bar{\mathbf{k}}\mathbf{q}}(t) \mathbf{h}_{\bar{\mathbf{k}}(\bar{\mathbf{k}}+\mathbf{q})}(t) \\ & + 2 \sum_{\mathbf{k}'} \left[ \mathcal{G}^{\mathbf{k}\bar{\mathbf{k}}\mathbf{q}}(t) \mathcal{V}^{(-\mathbf{q})\mathbf{k}'(\bar{\mathbf{k}}+\mathbf{q})} \rho_{\bar{\mathbf{k}}(\bar{\mathbf{k}}+\mathbf{q})}^{\Delta}(t) - \rho_{(\bar{\mathbf{k}}-\mathbf{q})\mathbf{k}}^{\Delta}(t) \mathcal{V}^{(-\mathbf{q})(\mathbf{k}-\mathbf{q})\mathbf{k}'} \mathcal{G}^{\mathbf{k}'\bar{\mathbf{k}}\mathbf{q}}(t) \right] \equiv \mathcal{I}^{\mathbf{k}\bar{\mathbf{k}}\mathbf{q}}(t). \end{aligned} \quad (5)$$

In Eq. (5)  $\rho_{\mathbf{k}\bar{\mathbf{k}}'}^{\Delta} \equiv \rho_{\mathbf{k}\bar{\mathbf{k}}'}^{\lessgtr} - \rho_{\mathbf{k}\bar{\mathbf{k}}'}^{\lessgtr}$ , and matrix multiplication between  $N_b^2 \times N_b^2$  matrices is understood.

Equations (1,4,5) form a closed system of ODE that is equivalent to the original  $GW$ -GKBA scheme. Notice that in the  $GW$ -ODE scheme the  $GW$  self-energy  $\Sigma(t, t')$  is never evaluated. The collision integral  $\mathcal{I}(t)$  depends only on the instantaneous  $\mathcal{G}(t)$ ,  $\rho(t)$  and  $\mathbf{h}(t)$ . The numerical scaling is linear in time, quartic with the number of  $\mathbf{k}$  points and sextic with the number of bands. The second-Born (2B) approximation without the second-order exchange contribution is recovered by neglecting the last line of Eq. (5). If we instead set  $N_b = 1$  and choose  $V_{1111}^{\mathbf{q}\bar{\mathbf{k}}\mathbf{k}'} = V^{\mathbf{q}}$  depending only on the transferred momentum  $\mathbf{q}$ , Eqs. (1,4,5) reduce to the  $GW$ -ODE for jellium [17, 18].

We have implemented the  $GW$ -ODE scheme in 2D systems having a single valence ( $i = 1$ ) and a single conduction ( $i = 2$ ) band (hence  $N_b = 2$ ). Accordingly, the equilibrium one-particle density matrix  $\rho_{\mathbf{k}11}^{\text{eq}} = 1$ ,  $\rho_{\mathbf{k}22}^{\text{eq}} = 0$ , and  $\rho_{\mathbf{k}12}^{\text{eq}} = 0$ . We use  $\rho_{\mathbf{k}}(0) = \rho_{\mathbf{k}}^{\text{eq}}$  as initial condition. To avoid double countings we also subtract from the right

hand side of Eq. (5) the contribution of initial correlations, already taken into account in the dressing the  $GW$  band structures  $\epsilon_{\mathbf{k}i}$ . Hence we modify the equation of motion for  $\mathcal{G}$  according to  $i\frac{d}{dt}\mathcal{G}^{\mathbf{k}\bar{\mathbf{k}}\mathbf{q}}(t) = \mathcal{I}^{\mathbf{k}\bar{\mathbf{k}}\mathbf{q}}(t) - \mathcal{I}^{\mathbf{k}\bar{\mathbf{k}}\mathbf{q}}(0)$  and set  $\mathcal{G}^{\mathbf{k}\bar{\mathbf{k}}\mathbf{q}}(0) = 0$ . Although the equilibrium state is weakly correlated, the electron-electron interaction plays a crucial role in the photo-excited dynamics, see below. We solve numerically the  $GW$ -ODE equations for the  $GW$  and 2B approximations using the CHEERS code [34]; we also provide comparisons with results from the BE, i.e., the semiconductor Bloch equation [35] in the 2B-Markov approximation [33].

*Carrier multiplication in photo-excited graphene* – Due to its semimetallic nature pristine graphene has scarce screening efficiency [36, 37]. Moreover in Ref. [38] it has been shown that second-order exchange effects are negligible. We therefore expect that 2B and  $GW$  calculations give similar results and that the comparison between  $GW$  and BE well highlights the role of non-Markovian effects.

Previous studies have shown that immediately after the photoexcitation, the electron dynamics is dominated by the impact

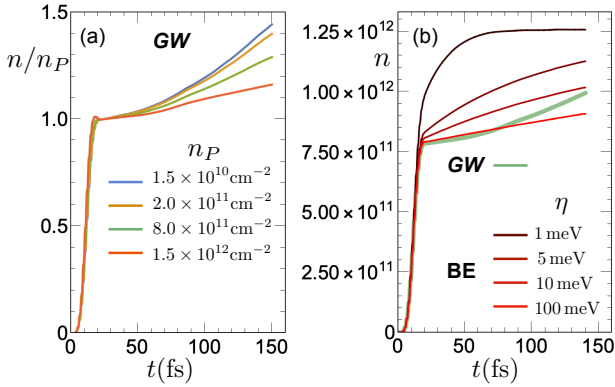


FIG. 2. (a) Time-dependent normalized carrier density  $n(t)/n_P$  in photo-excited graphene in the  $GW$  approximation for different pump intensities. (b) Carrier density  $n(t)$  in the  $GW$  and BE approach for different values of the broadening  $\eta$ ; in all simulations we use the same pump intensity, giving  $n_P = 8 \times 10^{11} \text{cm}^{-2}$  in the  $GW$  case.

ionization [21, 24, 39–42]. This inter-band process promotes electrons from the valence to the conduction band at the expense of energy loss by photo-excited hot carriers. Due to the linearity of the Dirac spectrum, carrier multiplication can occur mainly via *collinear scattering* [41]. These scatterings, however, have a vanishingly small phase-space (and therefore become irrelevant) if the energy of the quasiparticles is exactly conserved [41]. This means that in the BE approach an empirical energy-broadening  $\eta$  [33] must be introduced to capture the effect.

For photoexcitations with photon energy  $\lesssim 3 \text{ eV}$  graphene is well described by the Dirac cone approximation [43], where conduction and valence bands have linear dispersion  $\epsilon_{k1,2} = \pm v_F k$ , with  $v_F$  the Fermi velocity and  $k = |\mathbf{k}|$  a small momentum around the K (K') point of the first Brillouin zone. In this case the Coulomb integral has a simple expression [43]  $V_{lnmi}^{\mathbf{q}\mathbf{k}\mathbf{k}'} = \frac{2\pi}{\epsilon q} F_{il}(\theta_{\mathbf{k}-\mathbf{q}} - \theta_{\mathbf{k}}) F_{mn}(\theta_{\mathbf{k}'+\mathbf{q}} - \theta_{\mathbf{k}'})$ , where  $F_{\alpha\beta}(\theta) = \frac{1+(-1)^{\alpha+\beta} e^{i\theta}}{2}$ , with  $\theta_{\mathbf{k}}$  the polar angle of the momentum  $\mathbf{k}$ . We take a dielectric constant  $\epsilon \approx 2.5$ , originating from a typical insulating substrate like  $\text{SiO}_2$  [44].

We consider graphene initially in the ground state and then driven out of equilibrium by a pump field linearly polarized along a direction  $\mathbf{e}$  on the plane. The explicit form of the light-matter interaction term is [45]  $P_{\mathbf{k}ij}(t) = \delta_{i1}\delta_{j2} M E(t) \frac{k_x e_y - k_y e_x}{k}$ , where the  $E(t) = \theta(1 - |1 - 2t/T_P|) E \sin^2\left(\frac{\pi t}{T_P}\right) \sin(\omega_P t)$  is the pump envelope with duration  $T_P = 20 \text{ fs}$  and frequency  $\omega_P = 1.5 \text{ eV}$ ; the Rabi frequency  $M$  is varied in order to promote excitation densities in the range  $10^{10} - 10^{12} \text{ carriers/cm}^2$ . To improve convergence we have regularized the bare interaction  $1/q \rightarrow 1/(q + q_c)$ ; in the simulations  $q_c = 0.01 \text{ \AA}^{-1}$  is a small cutoff that can be understood as the Thomas-Fermi momentum ascribed to a small unintentional doping [46]. The EOM have been solved numerically by simulating the carrier dynamics inside the K (K') valley up to a time 150 fs. At times  $\gtrsim 200 \text{ fs}$  intervalley scat-

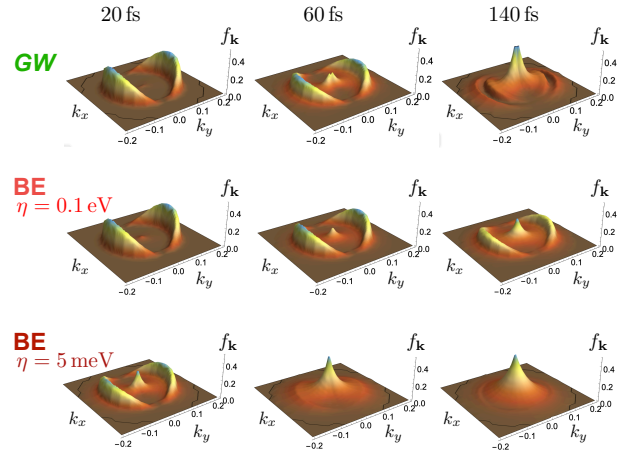


FIG. 3. Snapshots of the carrier distribution function  $f_{\mathbf{k}}$  in photo-excited graphene in  $GW$  (1st row), BE for  $\eta = 100 \text{ meV}$  (2nd row) and BE  $\eta = 5 \text{ meV}$  (3rd row). Here the pump field is polarized along the  $x$  axis. Momenta  $k_x$  and  $k_y$  are in  $\text{\AA}^{-1}$ .

tering and electron-phonon interactions (which are neglected in our calculations) start to be relevant [40, 41] and our theory becomes less accurate. In Fig. 2a we show the evolution of the carrier density in the conduction band  $n(t) = \frac{4}{A} \sum_{\mathbf{k}} \rho_{\mathbf{k}22}(t)$  during and after the illumination, for different pump intensities. The factor 4 accounts for the spin and valley degeneracy while  $A = 5.1 \times 10^{-16} \text{cm}^2$  is the unit-cell area of graphene. In order to illustrate the carrier multiplication effect as a function of the pump intensity we plot  $n(t)/n_P$ , where  $n_P \equiv n(T_P)$  is the excited density at the end of the pump. The  $GW$  simulation confirms the predicted behavior that the rate of carrier multiplication decreases by increasing the carrier density [21]. This is due to a Pauli blocking effect that reduces the phase-space for impact ionization. Notice that no parameters (like  $\eta$  in the BE approach) appear in the  $GW$ -ODE scheme.

In Fig. 2b we compare the  $GW$  result to the BE outcome for different values of the broadening  $\eta$ . In all simulations we use the same pump intensity, giving  $n_P = 8 \times 10^{11} \text{cm}^{-2}$  in the  $GW$  case. We see that the carrier multiplication effect predicted by the BE approach depends strongly on the chosen broadening. During illumination, energy is not conserved and therefore the smaller  $\eta$  is, the less accurate is the description of the early transient dynamics for  $t < T_P$ . This explains why at the beginning the BE curve obtained with the large value  $\eta = 0.1 \text{ eV}$  is the closest to the  $GW$  one. At larger times  $t \gtrsim 60 \text{ fs}$ , however the two curves depart from each other. In particular the  $GW$  evolution does not follow (at least within this temporal window) the typical exponential saturation behavior of the BE, characterized by a downward concavity for  $t > T_P$ . This qualitative difference is due to non Markovian effects as in this case the 2B results (not shown) are very close to the  $GW$  one.

In Fig. 3 we compare the evolution of the momentum-resolved occupations  $f_{\mathbf{k}}(t) = \rho_{\mathbf{k}22}(t)$  in different approaches.

We clearly see that the carrier population is initially highly anisotropic due to the linear polarization of the pulse [40]. As already observed *GW* agrees well with BE for  $\eta = 0.1$  eV up to time  $t \approx 60$  fs, i.e., when the distribution is still anisotropic. At this time a substantial portion of the initial hot electrons have already migrated towards the Dirac point due to inter-particle scattering. At larger times *GW* predicts a rapid thermalization while in BE the same process is much slower. The BE results are strongly affected by the value of  $\eta$ . At smaller  $\eta = 5$  meV the thermalization is very fast: there is a sizable charge redistribution already during illumination, and at  $t \approx 60$  fs the distribution is essentially isotropic.

A crucial feature of the real-time *GW* method is the updating of the screened interaction during the time evolution. We highlight this effect in a prototype 2D semiconductor hosting bound excitons inside the gap, and study the dynamics activated by pumping in resonance with the lowest excitonic energy. A fluid of coherent excitons is then formed [47], characterized by long-lived coherent oscillations of the macroscopic polarization [48–54]. We here address the relaxation dynamics of the macroscopic polarization due to excited state screening. Let us model a direct-gap 2D semiconductor with band dispersions  $\epsilon_{\mathbf{k}1,2} = \pm\epsilon_g/2 \pm k^2/2m$ , where  $\epsilon_g$  is the bandgap and  $m$  the effective mass of electrons and holes. In semiconductors the Coulomb integrals that do not conserve the particle number in each band are typically small [55] and can be neglected. In addition we assume a dependence only on the transferred momentum, i.e.  $V_{lnmi}^{\mathbf{q}\mathbf{k}_1\mathbf{k}_2} = V^{\mathbf{q}}\delta_{li}\delta_{nm}$ , and take the standard 2D interaction  $V^{\mathbf{q}} = 2\pi/\epsilon(q + q_c)$ , where  $\epsilon$  accounts for the dielectric screening of the surrounding environment and  $q_c$  encodes the ground state screening from the filled bands. Typical values to describe optical excitation in a monolayer transition metal dichalcogenide (TMD) around the K valley are  $\epsilon_g = 2$  eV,  $m = 0.5m_e$  ( $m_e$  being the electron mass) and  $\epsilon = 10$  (e.g. sapphire substrate). By solving the Bethe-Salpeter equation at equilibrium with these parameters we find the lowest energy exciton at  $\epsilon_x \approx 1.9$  eV (i.e. binding energy of 0.1 eV).

The system is excited with a laser pulse having the same envelope  $E(t)$  used for graphene but with a resonant frequency  $\omega_P = \epsilon_x = 1.9$  eV and duration  $T_P = 25$  fs. For simplicity we assume an isotropic excitation with momentum-independent light-matter interaction  $P_{\mathbf{k}ij}(t) = \delta_{i1}\delta_{j2}ME(t)$ . Accordingly the density matrix and all observables depend only on the modulus  $k$ . Also in this case the Rabi frequency is varied in order to promote excitation densities in the range  $10^{10} - 10^{12}$  carriers/cm<sup>2</sup>. In Fig.4(a) we show the evolution of the momentum-resolved carrier distribution  $f_k(t) = \rho_{k22}(t)$  for a low excited density  $n_P = \frac{4}{A} \sum_{\mathbf{k}} \rho_{k22}(T_P) = 10^{11}$  cm<sup>-2</sup> – the characteristic value  $A = 9 \times 10^{-16}$  cm<sup>2</sup> has been used. During pumping excitons are predominantly created and  $f_k \propto |Y_k|^2$ , where  $Y_k$  is the exciton wavefunction [29, 30, 54, 56, 57]. We have recently shown that for small excited densities the coherent exciton superfluid is not able to screen the Coulomb interaction [58]. As a consequence the  $e$ - $h$  attraction is not reduced and excitons survive

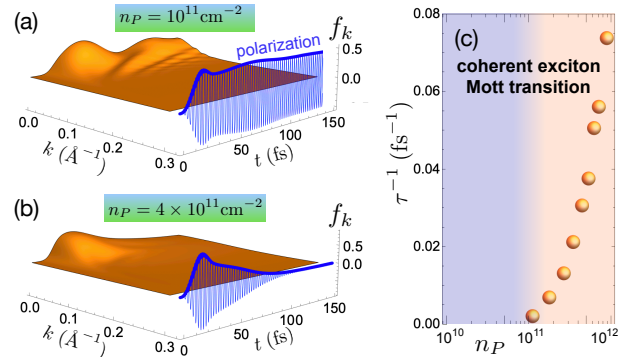


FIG. 4. Real-time *GW* evolution of the carrier distribution function  $f_k(t)$  in a 2D semiconductor for excitation density  $n_P = 10^{11}$  cm<sup>-2</sup> (a) and  $n_P = 4 \times 10^{11}$  cm<sup>-2</sup> (b). The time-dependent polarization  $p(t)$  (multiplied by a factor 2000) is also shown as a blue curve. In panel c we display the polarization inverse lifetime  $\tau^{-1}$  as a function of  $n_P$ . Here we used  $q_c = 0.02$  Å<sup>-1</sup>.

for long time. The superfluid phase is characterized by a macroscopic polarization  $p(t) = \sum_{\mathbf{k}} \rho_{k12}(t)$  that oscillates monochromatically at the exciton frequency  $\epsilon_x$  [54], see the blue curve in Fig.4(a). In this regime no relaxation occurs, and the carrier occupations  $f_k(t)$  slowly attain the values reached at the end of the pump. The system can eventually thermalize only at later times via electron-phonon scattering [59] (not considered in the present work).

The scenario changes dramatically at higher excited densities. In Fig. 4b we see that for  $n_P = 4 \times 10^{11}$  cm<sup>-2</sup> the polarization damps in about 100 fs, and after few femtoseconds ( $t \gtrsim 150$  fs) the occupations  $f_k$  reach steady-state values describing a Fermi-Dirac distribution at temperature  $\sim 2000$  K (not shown), consistently with recent data [60]. We have systematically studied the lifetime of the polarization  $p(t)$  by varying the excitation density. In Fig. 4 we plot the inverse of the time  $\tau$  needed to reduce the amplitude of  $p(t)$  by one order of magnitude, as function of the carrier density  $n_P$ . We see that no damping of the polarization can be detected for  $n_P \lesssim 10^{11}$  cm<sup>-2</sup>, while  $\tau^{-1}$  grows very fast beyond this threshold. The mechanism behind this behavior is a screening cascade: (1) at sufficiently high excitation density the screening of the excitonic superfluid is nonvanishing and the effective  $e$ - $h$  attraction is reduced (2) excitons start dissociating in a plasma of quasi-free electrons in conduction band and quasi-free holes in valence band (3) the  $e$ - $h$  plasma has a high screening efficiency and the  $e$ - $h$  attraction gets drastically reduced [57]. This self-sustained mechanism leads to a rapid melting of the superfluid state, signaled by a decay of the polarization. The thermalization occurs via scattering between incoherent quasiparticles, and the occupations  $f_k(t)$  relax towards a hot Fermi-Dirac distribution. We emphasize that this *coherent exciton Mott transition* is different from the well-known excitonic Mott transition [61–64] which refers to the breakdown of a system of incoherent excitons [65].

In conclusion we have demonstrated the feasibility of real-time *GW* simulations in 2D materials via the generalization



and practical implementation of the recently proposed  $GW$ -ODE scheme [17, 18]. The  $GW$  approximation gives easy access to so far neglected effects that we show are crucial for the photo-excited many-electrons dynamics in graphene and 2D semiconductors. Although the method presented in this work is devoted to purely electronic processes, it can be complemented with electron-phonon scatterings without affecting the linear-time scaling [19]. This opens new avenues for the *ab initio* description and understanding of ultrafast phenomena observed in time-resolved experiments.

*Acknowledgements* We acknowledge funding from MIUR PRIN Grant No. 20173B72NB and from INFN17-Nemesys project. G.S. acknowledges Tor Vergata University for financial support through the Mission Sustainability Project 2DU-TOPI.

- 
- [1] L. Hedin, New method for calculating the one-particle green's function with application to the electron-gas problem, *Phys. Rev.* **139**, A796 (1965).
- [2] L. Reining, The  $GW$  approximation: content, successes and limitations, *Wiley Interdisciplinary Reviews: Computational Molecular Science* **8**, e1344 (2018).
- [3] D. Golze, M. Dvorak, and P. Rinke, The  $GW$  compendium: A practical guide to theoretical photoemission spectroscopy, *Frontiers in Chemistry* **7**, 377 (2019).
- [4] L. P. Kadanoff and G. A. Baym, *Quantum statistical mechanics: Green's function methods in equilibrium and nonequilibrium problems* (Benjamin, 1962).
- [5] G. Stefanucci and R. van Leeuwen, *Nonequilibrium Many-Body Theory of Quantum Systems: A Modern Introduction* (Cambridge University Press, Cambridge, 2013).
- [6] K. Balzer and M. Bonitz, *Nonequilibrium Green's Functions Approach to Inhomogeneous Systems* (Springer, 2012).
- [7] P. Myöhänen, A. Stan, G. Stefanucci, and R. van Leeuwen, Kadanoff-Baym approach to quantum transport through interacting nanoscale systems: From the transient to the steady-state regime, *Phys. Rev. B* **80**, 115107 (2009).
- [8] P. Myöhänen, A. Stan, G. Stefanucci, and R. van Leeuwen, A many-body approach to quantum transport dynamics: Initial correlations and memory effects, *EPL (Europhysics Letters)* **84**, 67001 (2008).
- [9] M. Puig von Friesen, C. Verdozzi, and C.-O. Almbladh, Kadanoff-Baym dynamics of hubbard clusters: Performance of many-body schemes, correlation-induced damping and multiple steady and quasi-steady states, *Phys. Rev. B* **82**, 155108 (2010).
- [10] M. P. von Friesen, C. Verdozzi, and C.-O. Almbladh, Successes and failures of Kadanoff-Baym dynamics in Hubbard nanoclusters, *Phys. Rev. Lett.* **103**, 176404 (2009).
- [11] M. Schüler, J. Berakdar, and Y. Pavlyukh, Time-dependent many-body treatment of electron-boson dynamics: Application to plasmon-accompanied photoemission, *Phys. Rev. B* **93**, 054303 (2016).
- [12] D. Golež, M. Eckstein, and P. Werner, Multiband nonequilibrium  $GW$  + EDMFT formalism for correlated insulators, *Phys. Rev. B* **100**, 235117 (2019).
- [13] P. Lipavský, V. Špička, and B. Velický, Generalized Kadanoff-Baym ansatz for deriving quantum transport equations, *Phys. Rev. B* **34**, 6933 (1986).
- [14] L. Bányai, Q. T. Vu, B. Mieck, and H. Haug, Ultrafast quantum kinetics of time-dependent RPA-screened Coulomb scattering, *Phys. Rev. Lett.* **81**, 882 (1998).
- [15] Q. T. Vu, H. Haug, W. A. Hügel, S. Chatterjee, and M. Wegener, Signature of electron-plasmon quantum kinetics in gaas, *Phys. Rev. Lett.* **85**, 3508 (2000).
- [16] Q. T. Vu and H. Haug, Time-dependent screening of the carrier-phonon and carrier-carrier interactions in nonequilibrium systems, *Phys. Rev. B* **62**, 7179 (2000).
- [17] N. Schlünzen, J.-P. Joost, and M. Bonitz, Achieving the scaling limit for nonequilibrium green functions simulations, *Phys. Rev. Lett.* **124**, 076601 (2020).
- [18] J.-P. Joost, N. Schlünzen, and M. Bonitz, G1-G2 scheme: Dramatic acceleration of nonequilibrium green functions simulations within the hartree-fock generalized kadanoff-baym ansatz, *Phys. Rev. B* **101**, 245101 (2020).
- [19] D. Karlsson, R. van Leeuwen, Y. Pavlyukh, E. Perfetto, and G. Stefanucci, Fast Green's function method for ultrafast electron-boson dynamics, *Phys. Rev. Lett.* **127**, 036402 (2021).
- [20] Y. Pavlyukh, E. Perfetto, and G. Stefanucci, Photoinduced dynamics of organic molecules using nonequilibrium Green's functions with second-Born,  $GW$ ,  $T$ -matrix, and three-particle correlations, *Phys. Rev. B* **104**, 035124 (2021).
- [21] T. Winzer, A. Knorr, and E. Malic, Carrier multiplication in graphene, *Nano Letters* **10**, 4839 (2010).
- [22] J. C. W. Song, K. J. Tielrooij, F. H. L. Koppens, and L. S. Levitov, Photoexcited carrier dynamics and impact-excitation cascade in graphene, *Phys. Rev. B* **87**, 155429 (2013).
- [23] D. Brida, A. Tomadin, C. Manzoni, Y. J. Kim, A. Lombardo, S. Milana, R. R. Nair, K. S. Novoselov, A. C. Ferrari, G. Cerullo, *et al.*, Ultrafast collinear scattering and carrier multiplication in graphene, *Nat. commun.* **4**, 1 (2013).
- [24] T. Plötzing, T. Winzer, E. Malic, D. Neumaier, A. Knorr, and H. Kurz, Experimental verification of carrier multiplication in graphene, *Nano letters* **14**, 5371 (2014).
- [25] K. Tielrooij, J. Song, S. A. Jensen, A. Centeno, A. Pesquera, A. Z. Elorza, M. Bonn, L. Levitov, and F. Koppens, Photoexcitation cascade and multiple hot-carrier generation in graphene, *Nature Physics* **9**, 248 (2013).
- [26] S. Tani, F. m. c. Blanchard, and K. Tanaka, Ultrafast carrier dynamics in graphene under a high electric field, *Phys. Rev. Lett.* **109**, 166603 (2012).
- [27] J. C. Johannsen, S. Ulstrup, A. Crepaldi, F. Cilento, M. Zaccagna, J. A. Miwa, C. Cacho, R. T. Chapman, E. Springate, F. Fromm, *et al.*, Tunable carrier multiplication and cooling in graphene, *Nano letters* **15**, 326 (2015).
- [28] M. Dendzik, R. P. Xian, E. Perfetto, D. Sangalli, D. Kutnyakhov, S. Dong, S. Beaulieu, T. Pincelli, F. Pressacco, D. Curcio, S. Y. Agustsson, M. Heber, J. Hauer, W. Wurth, G. Brenner, Y. Acremann, P. Hofmann, M. Wolf, A. Marini, G. Stefanucci, L. Rettig, and R. Ernstorfer, Observation of an excitonic Mott transition through ultrafast core-cum-conduction photoemission spectroscopy, *Phys. Rev. Lett.* **125**, 096401 (2020).
- [29] M. K. Man, J. Madéo, C. Sahoo, K. Xie, M. Campbell, V. Pareek, A. Karmakar, E. L. Wong, A. Al-Mahboob, N. S. Chan, *et al.*, Experimental measurement of the intrinsic excitonic wave function, *Science Advances* **7**, eabg0192 (2021).
- [30] S. Dong, M. Puppini, T. Pincelli, S. Beaulieu, D. Christiansen, H. Hübener, C. W. Nicholson, R. P. Xian, M. Dendzik, Y. Deng, *et al.*, Direct measurement of key exciton properties: Energy,

- dynamics, and spatial distribution of the wave function, *Natural Sciences*, e10010 (2021).
- [31] Z. Nie, R. Long, L. Sun, C.-C. Huang, J. Zhang, Q. Xiong, D. W. Hewak, Z. Shen, O. V. Prezhdo, and Z.-H. Loh, Ultrafast carrier thermalization and cooling dynamics in few-layer MoS<sub>2</sub>, *ACS nano* **8**, 10931 (2014).
- [32] E. Perfetto, D. Sangalli, A. Marini, and G. Stefanucci, Nonequilibrium Bethe-Salpeter equation for transient photoabsorption spectroscopy, *Phys. Rev. B* **92**, 205304 (2015).
- [33] See Supplemental Material for details on the index convention, derivation of the ODE scheme, derivation of the BE scheme, and numerical implementation.
- [34] E. Perfetto and G. Stefanucci, Cheers: a tool for correlated hole-electron evolution from real-time simulations, *J. Phys. Condens. Matter* **30**, 465901 (2018).
- [35] M. Kira and S. Koch, Many-body correlations and excitonic effects in semiconductor spectroscopy, *Progress in Quantum Electronics* **30**, 155 (2006).
- [36] J. González, F. Guinea, and M. A. H. Vozmediano, Unconventional quasiparticle lifetime in graphite, *Phys. Rev. Lett.* **77**, 3589 (1996).
- [37] E. H. Hwang, B. Y.-K. Hu, and S. Das Sarma, Inelastic carrier lifetime in graphene, *Phys. Rev. B* **76**, 115434 (2007).
- [38] Y. Pavlyukh, G. Stefanucci, and R. van Leeuwen, Dynamically screened vertex correction to *GW*, *Phys. Rev. B* **102**, 045121 (2020).
- [39] F. Rana, Electron-hole generation and recombination rates for coulomb scattering in graphene, *Phys. Rev. B* **76**, 155431 (2007).
- [40] E. Malic, T. Winzer, E. Bobkin, and A. Knorr, Microscopic theory of absorption and ultrafast many-particle kinetics in graphene, *Phys. Rev. B* **84**, 205406 (2011).
- [41] A. Tomadin, D. Brida, G. Cerullo, A. C. Ferrari, and M. Polini, Nonequilibrium dynamics of photoexcited electrons in graphene: Collinear scattering, Auger processes, and the impact of screening, *Phys. Rev. B* **88**, 035430 (2013).
- [42] G. Alymov, V. Vyurkov, V. Ryzhii, A. Satou, and D. Svintsov, Auger recombination in dirac materials: A tangle of many-body effects, *Phys. Rev. B* **97**, 205411 (2018).
- [43] A. H. Castro Neto, F. Guinea, N. M. R. Peres, K. S. Novoselov, and A. K. Geim, The electronic properties of graphene, *Rev. Mod. Phys.* **81**, 109 (2009).
- [44] T. Ando, Screening effect and impurity scattering in monolayer graphene, *J. Phys. Soc. Japan* **75**, 074716 (2006).
- [45] A. Grüneis, R. Saito, G. G. Samsonidze, T. Kimura, M. A. Pimenta, A. Jorio, A. G. S. Filho, G. Dresselhaus, and M. S. Dresselhaus, Inhomogeneous optical absorption around the K point in graphite and carbon nanotubes, *Phys. Rev. B* **67**, 165402 (2003).
- [46] E. H. Hwang and S. Das Sarma, Dielectric function, screening, and plasmons in two-dimensional graphene, *Phys. Rev. B* **75**, 205418 (2007).
- [47] S. Schmitt-Rink, D. S. Chemla, and H. Haug, Nonequilibrium theory of the optical Stark effect and spectral hole burning in semiconductors, *Phys. Rev. B* **37**, 941 (1988).
- [48] J. R. Kuklinski and S. Mukamel, Optical properties of wannier excitons in the linear and weakly nonlinear regime, *Phys. Rev. B* **42**, 2959 (1990).
- [49] S. Glutsch and R. Zimmermann, Coherent optics for pumping near the absorption edge, *Phys. Rev. B* **45**, 5857 (1992).
- [50] P. Littlewood and X. Zhu, Possibilities for exciton condensation in semiconductor quantum-well structures, *Phys. Scr.* **1996**, 56 (1996).
- [51] T. Östreich and K. Schönhammer, Non-stationary excitonic-insulator states in photoexcited semiconductors, *Zeitschrift für Physik B Condensed Matter* **91**, 189 (1993).
- [52] K. Hannewald, S. Glutsch, and F. Bechstedt, Excitonic insulator through coherent pulse excitation?, *Journal of Physics: Condensed Matter* **13**, 275 (2000).
- [53] S. Glutsch, F. Bechstedt, and R. Zimmermann, Optical excitation and bose condensation of excitons in low-dimensional systems, *physica status solidi (b)* **172**, 357 (1992).
- [54] E. Perfetto, D. Sangalli, A. Marini, and G. Stefanucci, Pump-driven normal-to-excitonic insulator transition: Josephson oscillations and signatures of BEC-BCS crossover in time-resolved ARPES, *Phys. Rev. Materials* **3**, 124601 (2019).
- [55] R. E. Groenewald, M. Rösner, G. Schönhoff, S. Haas, and T. O. Wehling, Valley plasmonics in transition metal dichalcogenides, *Phys. Rev. B* **93**, 205145 (2016).
- [56] E. Perfetto, S. Bianchi, and G. Stefanucci, Time-resolved arpes spectra of nonequilibrium excitonic insulators: Revealing macroscopic coherence with ultrashort pulses, *Phys. Rev. B* **101**, 041201 (2020).
- [57] E. Perfetto and G. Stefanucci, Ultrafast creation and melting of nonequilibrium excitonic condensates in bulk WSe<sub>2</sub>, *Phys. Rev. B* **103**, L241404 (2021).
- [58] E. Perfetto, A. Marini, and G. Stefanucci, Self-consistent screening enhances the stability of the nonequilibrium excitonic insulator phase, *Phys. Rev. B* **102**, 085203 (2020).
- [59] G. Stefanucci and E. Perfetto, From carriers and virtual excitons to exciton populations: Insights into time-resolved ARPES spectra from an exactly solvable model, *Phys. Rev. B* **103**, 245103 (2021).
- [60] Y. Li, W. Liu, Y. Wang, Z. Xue, Y.-C. Leng, A. Hu, H. Yang, P.-H. Tan, Y. Liu, H. Misawa, *et al.*, Ultrafast electron cooling and decay in monolayer WS<sub>2</sub> revealed by time- and energy-resolved photoemission electron microscopy, *Nano letters* **20**, 3747 (2020).
- [61] W. F. Brinkman and T. M. Rice, Electron-hole liquids in semiconductors, *Phys. Rev. B* **7**, 1508 (1973).
- [62] N. F. Mott, Metal-insulator transitions, *Contemporary Physics* **14**, 401 (1973).
- [63] T. Rice, The electron-hole liquid in semiconductors: Theoretical aspects (Academic Press, 1978) pp. 1 – 86.
- [64] N. F. Mott, The basis of the electron theory of metals, with special reference to the transition metals, *Proceedings of the Physical Society. Section A* **62**, 416 (1949).
- [65] A. Steinhoff, M. Florian, M. Rösner, G. Schönhoff, T. O. Wehling, and F. Jahnke, Exciton fission in monolayer transition metal dichalcogenide semiconductors, *Nat. Commun.* **8**, 1166 (2017).